AIAA JOURNAL
Vol. 38, No. 1, January 2000

Numerical Solution of Acoustic Propagation Problems Using Linearized Euler Equations

Christophe Bailly* and Daniel Juvé†
École Centrale de Lyon, 69131 Ecully CEDEX, France

Some numerical solutions of acoustic propagation problems using linearized Euler equations are studied. The two-dimensional Euler equations are linearized around a known stationary mean flow. The computed solution is obtained by using a dispersion-relation-preserving scheme in space, combined with a fourth-order Runge–Kutta algorithm in time. This numerical integration leads to very good results in terms of accuracy, stability, and low storage. The implementation of source terms in these equations is studied very carefully in various configurations, inasmuch as the final goal is to improve and to validate the stochastic noise generation and radiation model. In this approach, the turbulent velocity field is modeled by a sum of random Fourier modes through a source term in the linearized Euler equations to predict the noise from subsonic flows. The radiation of a point source in a subsonic and a supersonic uniform mean flow is investigated. The numerical estimates are shown to be in excellent agreement with the analytical solutions. Then, the emphasis is on the ability of the method to describe correctly the multipolar structure of aeroacoustic sources. The radiation of dipolar and quadrupolar extended sources is, thus, studied. Next, a typical problem in jet noise is considered with the propagation of acoustic waves in a sheared mean flow. The numerical solution compares favorably with ray tracing. Finally, a nonlinear formulation of Euler's equations is solved to limit the growth of instability waves excited by the acoustic source terms.

I. Introduction

SOUND generation and propagation in a turbulent flow is a difficult numerical problem.[1,2] Acoustic fluctuations are very small by comparison to the aerodynamic fields, and tremendous numerical difficulties must be overcome in a direct calculation, in particular for high Reynolds subsonic flows. Lighthill's analogy[3] is one of the classical approaches to solve this problem. The equations of motion are rewritten as an inhomogeneous wave equation:

$$\frac{\partial^2 \rho'}{\partial t^2} - c_\infty^2 \nabla^2 \rho' = \frac{\partial^2 T_{ij}}{\partial x_i \partial x_j} \tag{1}$$

where ρ' is the acoustic density fluctuation, c_∞ the ambient speed of sound, and T_{ij} Lighthill's tensor. This source term is usually expressed as a function of the aerodynamic field variables $T_{ij} \simeq \rho u_i u_j$, where ρ and u_i are the density and the velocity components, respectively. However, this formulation suffers from limitations because refraction effects are included in the source term. In addition, Green's function must be known to obtain an integral formulation. Hence, only simple geometric configurations can be studied when the turbulent velocity field is known or modeled. The case of the noise generated in a duct obstructed by a diaphragm is one of the most complex geometries investigated in the literature.[4]

The linearized Euler equations (LEEs) are a natural extension to Lighthill's analogy in computational aeroacoustics (CAA) and provide accurate numerical solutions by only dealing with perturbations. Refraction effects of sound waves induced by the mean flow are taken into account, and LEEs are easier to solve numerically than a third-order differential equation such as Lilley's wave equation.[5] Recent numerical studies have focused on a two-step calculation where the mean flowfield is provided by analytical, experimental, or Reynolds-averaged equations. Viswanathan and Sankar[6] and Mankbadi et al.[7] introduced disturbances into the flowfield to calculate instability-wave radiation for supersonic jet noise. Full Euler equations are solved in Ref. 6, whereas in Ref. 7 LEEs are used. Another hybrid method was proposed by Morris et al.,[8,9] where a very large eddy simulation provided the acoustic and fluctuating aerodynamic fields. A set of nonlinear disturbance equations is solved by using the Smagorinsky eddy viscosity model as turbulence closure. Rectangular and circular supersonic jets have been investigated with this approach. In the previous investigations, sound generation and propagation are simultaneously calculated to predict radiated noise inasmuch as large turbulence structures are the main noise sources of supersonic jets.[10] Noise generated by subsonic high Reynolds number flows is quite different. Hardin and Pope[11] performed a two-step calculation with an acoustic analogy to compute the sound generated by low Mach number flows. A two-step calculation is also carried out in the stochastic noise generation and radiation (SNGR) model. In the first step, a stationary mean flowfield is calculated by solving the Reynolds-averaged Navier–Stokes equations. Euler's equations are then linearized around this mean flow, and in a second step, these equations are solved with a turbulent source term on the right-hand side. In the SNGR model, a space–time turbulent velocity field was modeled by a sum of random Fourier modes. A first application was carried out to calculate the noise of an axisymmetric subsonic jet.[12–14] However, some difficulties remain concerning the axisymmetric calculation of the propagation because the acoustic sources are completely correlated in the azimuthal direction. The numerical algorithm relied on a weak formulation of the two-dimensional linear equations,[15] and an extension of this numerical method to a three-dimensional geometry would be difficult. Therefore, a full three-dimensional calculation using the SNGR model requires a new solver.

The aim of this study is to improve this approach using a new algorithm, described in Sec. II. In addition, the implementation of source terms in the linearized Euler equations is carefully investigated. The case of source radiation in a subsonic and a supersonic uniform mean flow is treated in Sec. III, and the numerical estimates are compared to analytical solutions. It is shown in Sec. IV that the multipolar nature of a source distribution is preserved in solving LEEs, a crucial point in aeroacoustics. Section V deals with propagation in a sheared mean flow, and the numerical solution is compared to ray tracing. Finally, a nonlinear formulation is developed in Sec. VI to limit the growth of instability waves that are also supported by the linearized equations.

Presented as Paper 98-2267 at the AIAA/CEAS 4th Aeroacoustics Conference, Toulouse, France, 2–4 June 1998; received 3 October 1998; revision received 10 May 1999; accepted for publication 18 May 1999.

*Assistant Professor, Laboratoire de Mécanique des Fluides et d'Acoustique, Centre National de la Recherche Scientifique UMR 5509, B.P. 163. Member AIAA.

†Professor, Laboratoire de Mécanique des Fluides et d'Acoustique, Centre National de la Recherche Scientifique UMR 5509, B.P. 163. Member AIAA.

II. Numerical Algorithm

A. Governing Equations

The density ρ', the velocity $\boldsymbol{u}' = (u', v')$, and the pressure p' represent small perturbations superimposed on a mean flow of density ρ_o, velocity $\boldsymbol{u}_0 = (u_0, v_0)$, and pressure p_0, respectively. The Euler equations linearized around a stationary mean flow may be written as[16]

$$\frac{\partial \boldsymbol{U}}{\partial t} + \frac{\partial \boldsymbol{E}}{\partial x} + \frac{\partial \boldsymbol{F}}{\partial y} + \boldsymbol{H} = \boldsymbol{S} \tag{2}$$

where $\boldsymbol{U} = [\rho', \rho_0 u', \rho_0 v', p']^T$ is the unknown vector and $\boldsymbol{E}$ and $\boldsymbol{F}$ are the two-dimensional flux vectors. The vector $\boldsymbol{H}$ contains terms related to the gradients of the mean flow, which are equal to zero when the mean flow is uniform. The vector $\boldsymbol{S}$ represents possible unsteady sources in the flow.

B. Numerical Scheme

All of the variables are made dimensionless with the following reference scales: Δx for the length scale, c_∞ for the velocity scale, $\Delta x / c_\infty$ for the timescale, ρ_∞ for the density scale, and $\rho_\infty c_\infty^2$ for the pressure scale, where $\Delta x = \Delta y$ is the mesh step size. The seven-point stencil, dispersion-relation-preserving (DRP) scheme of Tam and Webb[16] is used for the spatial flux derivations of system (2):

$$\frac{\partial \boldsymbol{U}_i}{\partial t} = -\sum_{l=-3}^{3} a_l(\boldsymbol{E}_{i+l,j} + \boldsymbol{F}_{i,j+l}) - \boldsymbol{H}_{i,j} + \boldsymbol{S}_{i,j}$$

These authors chose the coefficients[1,16] a_l of their spatial discretization by requiring that the effective wave number $\bar{k}$ provided by the finite difference scheme be a close approximation to the actual wave number. This optimized fourth-order scheme is better than a nonoptimized sixth-order scheme using the same seven-point stencil. By the use of the criterion $|k - \bar{k}| < 0.005$, the resolution for these standard central finite differences (CFDs) in terms of points per wavelength is summarized in Table 1. Note that 7 mesh points per wavelength are necessary for the DRP scheme of Tam and Webb[16]; the standard six-order scheme requires 10 mesh points per wavelength. In some cases it is necessary to remove spurious numerical oscillations due to nonlinearities or mismatches with the boundary conditions or the initial conditions. These short waves can be filtered by an artificial selective damping proposed by Tam and Shen.[17] The damping terms are added to the right side of system (2) to obtain

$$\boldsymbol{D}_{i,j} = -\frac{1}{R_s}\sum_{l=-3}^{3} d_l(\boldsymbol{U}_{i+l,j} + \boldsymbol{U}_{i,j+l})$$

where R_s is the mesh Reynolds number, which is usually taken in the interval [5; 10]. The notation $R_s = \infty$ designates a calculation without artificial damping. The coefficients[1,17] d_j are chosen to damp only the short waves and not the long waves corresponding to an accurate resolution of the DRP scheme. The Fourier transform of the damping function collapses to the Gaussian function $\exp\{-\ln 2[(k - \pi)/\sigma]^2\}$ with a half-width $\sigma = 0.2\pi$ for the linearized Euler equations. The time integration is performed by a four-step Runge–Kutta algorithm because of its high-stability limit and its low-storage requirement. The solution at time step $n + 1$ is obtained by the following algorithm: $\boldsymbol{U}_{i,j}^p = \boldsymbol{U}_{i,j}^n + \alpha_p \Delta t \boldsymbol{K}_{i,j}^{p-1}$ for $p = 1, \ldots, 3$, with $\boldsymbol{K}_{i,j}^0 = \boldsymbol{K}_{i,j}^n$. The last step is

$$\boldsymbol{U}_{i,j}^{n+1} = \boldsymbol{U}_{i,j}^n + \alpha_4 \Delta t(\boldsymbol{K}_{i,j}^3 + \boldsymbol{D}_{i,j}^n) \tag{3}$$

Table 1 Resolution of the CFD scheme and the DRP scheme using the criterion $|k - \bar{k}| < 0.005$

Scheme	Wave number	Wavelength
CFD second order	$k \le 0.30$	$\lambda \ge 21.3$
CFD fourth order	$k \le 0.67$	$\lambda \ge 9.3$
CFD sixth order	$k \le 0.96$	$\lambda \ge 6.6$
7-point DRP scheme	$k \le 1.16$	$\lambda \ge 5.4$

with

$$\boldsymbol{K}_{i,j}^k = -\sum_{l=-3}^{3} a_l(\boldsymbol{E}_{i+l,j}^k + \boldsymbol{F}_{i,j+l}^k) - \boldsymbol{H}_{i,j}^k + \boldsymbol{S}_{i,j}^k$$

$$\boldsymbol{D}_{i,j}^n = -\frac{1}{R_s}\sum_{l=-3}^{3} d_l(\boldsymbol{U}_{i+l,j}^n + \boldsymbol{U}_{i,j+l}^n)$$

The coefficients α_p are chosen to obtain fourth-order accuracy in time when the spatial operator is linear.[18] In this case, the stability limit corresponds to a Courant–Friedrichs–Lewy (CFL) number less than 1.73, and the accuracy limit is CFL < 0.73. Two other time-integration schemes have been investigated[19] in the case of a nonlinear propagation, but the differences between these time schemes are too small to be noticed.

C. Boundary Conditions

The boundary conditions are very important in CAA.[1] Indeed, because of the high quality of the numerical algorithm, any disturbance of small amplitude can propagate in the computational domain contaminating the numerical solution. The boundary conditions of Tam and Webb[16] are implemented because the radiation boundary condition for outgoing acoustic waves is based on an asymptotic solution of the LEEs. In polar coordinates (r, θ) centered at the source position, we have

$$\left[\frac{\partial}{\partial t} + V(\theta)\frac{\partial}{\partial r} + \frac{V(\theta)}{2r}\right]U = 0$$

when $r \to \infty$. V is the group velocity of acoustic waves used in geometrical acoustics, defined by

$$V = \boldsymbol{u}_0 \cdot \boldsymbol{e}_r + \sqrt{c_0^2 - (\boldsymbol{u}_0 \cdot \boldsymbol{e}_\theta)^2}$$

where $\boldsymbol{e}_r$ and $\boldsymbol{e}_\theta$ are the unit vectors in the r and θ directions. For an outflow boundary condition, the pressure disturbance is an acoustic fluctuation, which is not the case for the velocity and density disturbances. For these last two variables, Euler's equations are used. This yields a set of compatible first-order differential equations.[16] The spatial derivatives are computed with optimized backward difference stencils[10,16] for the three ghost points surrounding the computational domain.

For two-dimensional calculations, the code requires 4.7 μs per time step and per mesh point on a Cray C98. Several test problems may be found in the literature to evaluate numerical algorithms in CAA[20,21] and have been investigated[19] with numerical algorithm (3). In the next sections, the study focuses on the implementation of source terms in the LEEs.

III. Source Radiation in a Uniform Mean Flow

This section deals with the radiation of a source in a subsonic and a supersonic mean flow. The analytic solution is known for these two problems. A monopole source is implemented by using the vector $\boldsymbol{S}$ in system (2), which yields

$$\boldsymbol{S}(x, y, t) = f(x, y)\sin \omega t \times [1, 0, 0, 1]^T \tag{4}$$

where $f(x, y) = \epsilon \exp\{-\alpha[(x - x_s)^2 + (y - y_s)^2]\}$ with $\alpha = \ln 2/2$. The source term is made dimensionless with $[\rho_\infty c_\infty / \Delta x, 0, 0, \rho_\infty c_\infty^3 / \Delta x]^T$. The amplitude is taken as $\epsilon = 0.5$, and the angular frequency is $\omega = 2\pi/30$. The artificial mesh Reynolds number is $R_s = 10$, and the time step is given by the condition $\Delta t = 1/(1 + M)$, corresponding to a CFL number of 1. The source is located at $x_s = y_s = 0$ over the computational domain $-200 \le x, y \le 200$, yielding a regular mesh of 401 × 401 points, and the radiation boundary conditions are used because this problem deals with acoustic fluctuations only. The analytical solution is given by the convolution product $p(x, y, t) = f(x, y) * \mathrm{d}\mathcal{G}/\mathrm{d}t(x, y, t)$, where the two-dimensional Green function $\mathcal{G}$ is provided by expression (A3) in the Appendix. Figure 1 shows the time evolution of pressure isocontours for a subsonic mean flow at $M = 0.5$. The pressure profile along the axis $y = 0$ is plotted in Fig. 2 and is compared to the analytical solution. Two acoustic waves propagate upstream and downstream

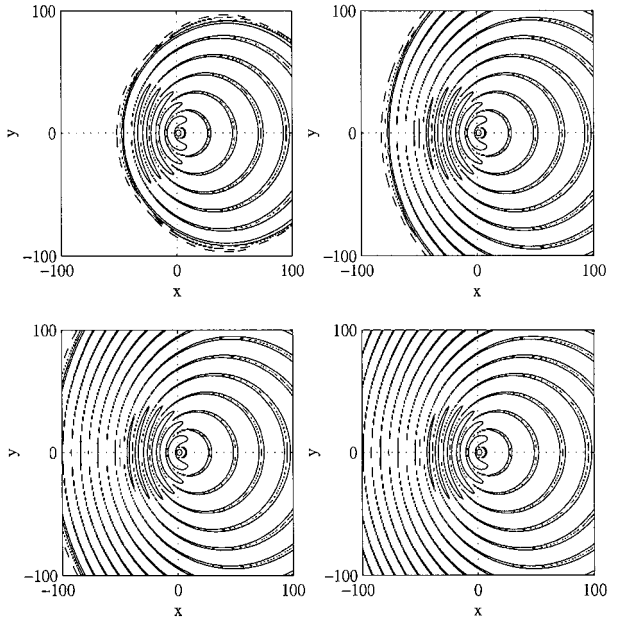

Fig. 1 Harmonic source in a uniform subsonic flow at $M = 0.5$: pressure isocontours at times $t = 90$, 150, 210, and 270 with the values ——, 10^{-1}, 10^{-2}, 10^{-3}; – – –, 10^{-4}; and · · ·, 10^{-5}.

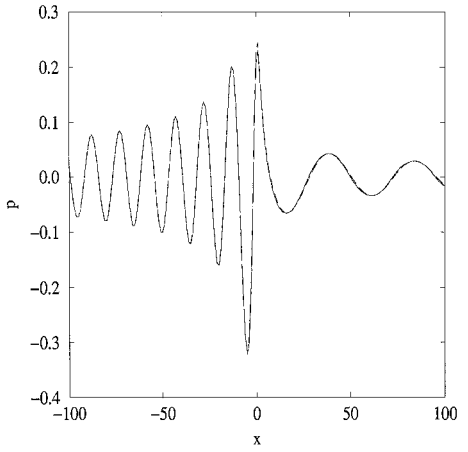

Fig. 2 Harmonic source in a uniform subsonic flow at $M = 0.5$ where pressure profile is plotted along axis $y = 0$ at time $t = 270$: ——, numerical solution, and – – –, analytical solution.

at the velocity $1 \pm M$ with an apparent wavelength $\lambda_c = (1 \pm M)\lambda$, where $\lambda = 30$. Excellent agreement is found between the computed pressure profile and the analytical solution. The supersonic case is investigated for Mach number $M = 1.5$ and a source located at $x_s = -50$ and $y_s = 0$. The calculation is performed with a higher selective damping $R_s = 4$ to remove small oscillations produced at the limits of the computational domain near the Mach cone. Indeed, there is a discontinuity of the boundary conditions due to the Mach cone defined by $M \sin\theta = 1$, that is, $\theta \simeq 41.8$ deg. This filtering is applied to short waves only, without consequence for resolved signals. Figure 3 shows the time evolution of pressure isocontours and the Mach cone. The radiated field is quite different from that of the subsonic case because both acoustic waves now propagate in the downstream direction at the velocity $M \pm 1$ and interfere with one another. The pressure profile along the axis $y = 0$ is plotted in Fig. 4 and is compared to the analytical solution obtained by a convolution product with the two-dimensional Green function [Eq. (A4)] defined in the Appendix. Good agreement between the calculation and the reference solution is again found except in the left-hand side of the source domain, for $x_s - 4 \leq x \leq x_s$. With reference to many other numerical tests, the problem could be attributed to the calculation of the convolution product of the analytical solution rather than the computed solution. These cases were previously examined by

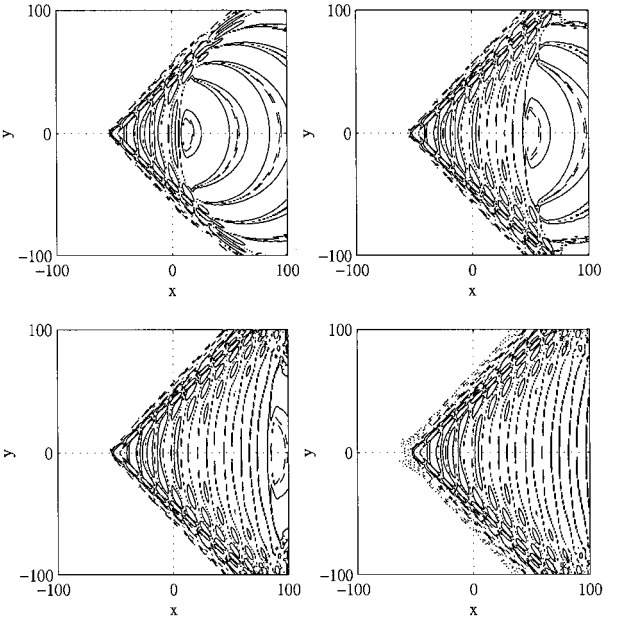

Fig. 3 Harmonic source in a uniform supersonic flow at $M = 1.5$: pressure isocontours at times $t = 114$, 190, 266, and 343 with the values ——, 10^{-1}, 10^{-2}; – – –, 10^{-3}; and · · ·, 10^{-4}.

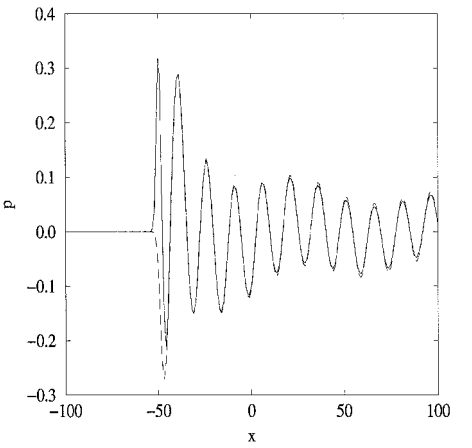

Fig. 4 Harmonic source in a uniform supersonic flow at $M = 1.5$; pressure profile is plotted along the axis $y = 0$ at time $t = 304$: ——, numerical solution, and – – –, analytical solution.

Candel and Crance,[22] and the present results are consistent with those obtained by Fourier synthesis.

IV. Definition of a Multipolar Source

The multipolar feature of a source $\boldsymbol{S}$ in system (2) is clearly identified by writing the wave equation corresponding to the LEEs. The LEEs take the simplified form

$$\frac{\partial \rho'}{\partial t} + \rho_0 \frac{\partial u_i'}{\partial x_i} = 0, \qquad \rho_0 \frac{\partial u_i'}{\partial t} + \frac{\partial p'}{\partial x_i} = S_i \tag{5}$$

for an homogeneous medium at rest, and the associated wave equation is

$$\frac{\partial^2 \rho'}{\partial t^2} - c_0^2 \nabla^2 \rho' = -\nabla \cdot \boldsymbol{S} \tag{6}$$

Thus, a dipole distribution $S_i = F_i$ in wave equation (6) is defined by

$$\int_V \frac{\partial F_i}{\partial x_i} \, \mathrm{d}\boldsymbol{x} = \int_S n_i F_i \, \mathrm{d}S = 0$$

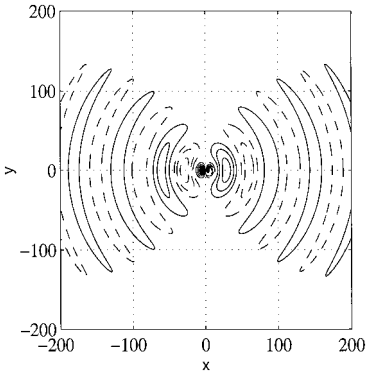

Fig. 5 Dipole distribution $S_i = F_i$; density isocontours at time $t = 640\Delta t$: ——, positive values, from 0.001 to 0.011 with a step size of 0.001; and · · ·, negative values.

with

$$\int_V F_i \, \mathrm{d}\boldsymbol{x} \neq 0$$

whereas a quadrupole distribution $S_i = \partial T_{ij}/\partial x_j$ is defined as

$$\int_V \frac{\partial^2 T_{ij}}{\partial x_i \partial x_j} \mathrm{d}\boldsymbol{x} = 0, \qquad \int_V \frac{\partial T_{ij}}{\partial x_j} \mathrm{d}\boldsymbol{x} = 0$$

With regard to aerodynamic noise applications, it is important to check that the solution of the LEEs preserves the multipolar nature of the sources. First, a dipole distribution F_i is investigated, given by

$$F_1 = \epsilon \cos[(\pi/10)x] e^{-\alpha y^2} \sin(\omega t), \qquad F_2 = 0$$

where $(x, y) \in [-5; 5] \times \mathbb{R}$. The angular frequency is taken as $\omega = 2\pi/60$, the amplitude of the source is $\epsilon = 0.01$, and the coefficient α is equal to $(\ell n\, 2)/5$. Figure 5 shows the density isocontours, and it appears that the dipole directivity is well illustrated. An accurate reference solution can be obtained in deriving the analytical solution. For the dipole distribution, wave equation (6) can be written as

$$\frac{\partial^2 \rho'}{\partial t^2} - c_0^2 \nabla^2 \rho' = -\nabla \cdot \boldsymbol{F}$$

where spatial derivatives of the source term (5) appear. Therefore, this problem is difficult for noise generation[23] because the size of the source domain is of the order of magnitude of the wavelength. The exact solution is given by the convolution product $\rho' = -F_1 \times \partial G/\partial x$, where Green's function is given by

$$G(\boldsymbol{x}, t) = \left\{ (i/4c_0^2) H_0^{(1)}[(\omega/c_0)r] \, e^{-i\omega t} \right\} \tag{7}$$

with $\boldsymbol{x} = (x, y)$ and $r = \sqrt{(x^2 + y^2)}$, and $H_0^{(1)}$ denotes the zeroth-order Hankel function of the first kind. A comparison between the calculated density profile along the axis $y = 0$ and the analytical solution is plotted in Fig. 6 at two instants. The acoustic field is calculated very accurately, without spurious oscillations near the source domain. For these computations, the mesh Reynolds number of the damping is $R_s = 5$, the computation domain is again $-200 \leq x, y \leq 200$, and the CFL number is 1. A quadrupole distribution T_{ij} in system (5) is also investigated. Its expression is chosen such that

$$T_{ij} = \begin{bmatrix} -\cos[(\pi/20)x] \, e^{-\alpha y^2} & 0 \\ 0 & \cos[(\pi/20)y] \, e^{-\alpha x^2} \end{bmatrix} \times \frac{20}{\pi} \epsilon \sin(\omega t)$$

in $(x, y) \in [-10; 10] \times [-10; 10]$; thus, the radiated field is now governed by the following wave equation:

$$\frac{\partial^2 \rho'}{\partial t^2} - c_0^2 \nabla^2 \rho' = -\nabla \cdot (\nabla \cdot \boldsymbol{T})$$

Figure 7 shows the acoustic field radiated by the quadrupole distribution, where the expected directivity is again well retrieved.

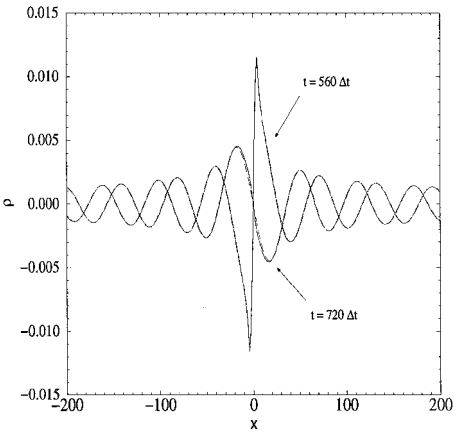

Fig. 6 Dipole distribution $S_i = F_i$; two density profiles are plotted along the axis $x_2 = 0$ at times $t = 560\Delta t$ and $720\Delta t$: ——, numerical solution, and - - - -, analytical solution.

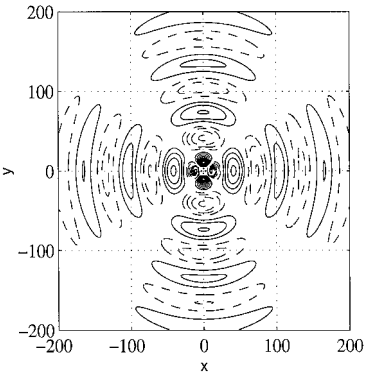

Fig. 7 Quadrupole distribution $S_i = \partial T_{ij}/\partial x_j$; density isocontours at time $t = 640\Delta t$: ——, positive values, from 0.001 to 0.011 with a step size of 0.001; and - - - -, negative values.

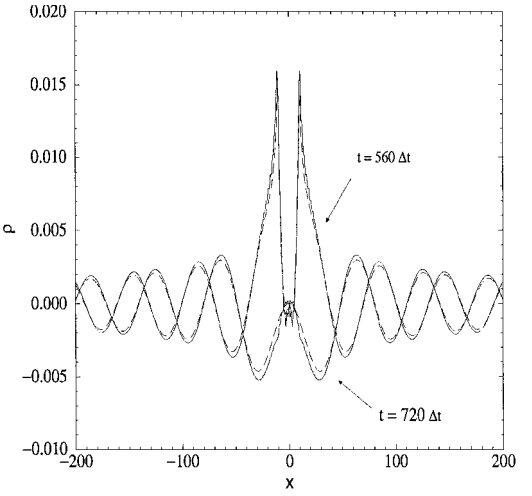

Fig. 8 Quadrupole distribution $S_i = \partial T_{ij}/\partial x_j$; two density profiles are plotted along the axis $x_2 = 0$ at times $t = 560\Delta t$ and $720\Delta t$: ——, numerical solution and - - - -, analytical solution.

The analytical solution takes the form of a sum of two convolution products

$$\rho' = -\frac{\partial T_{xx}}{\partial x} * \frac{\partial G}{\partial x} - \frac{\partial T_{yy}}{\partial y} * \frac{\partial G}{\partial y}$$

where Green's function is given by expression (7). Two comparisons between computations and the exact solution are shown in Fig. 8. Unlike the dipole distribution, small oscillations near the source are present. Indeed, in the quadrupole distribution, the source term in system (5) is not zero on the boundaries. Another test has been carried out in setting the source term $S_i = \partial T_{ij}/\partial x_j$ in a

two-dimensional jet. The multipolar nature of the source is again clearly identifiable.[24]

It is shown in this section that the multipolar nature of source distributions is preserved by LEEs. This is important because LEEs have to use this property to define multipolar turbulent sources. In the following two sections, propagation in a sheared mean flow is investigated. We know that three modes are supported by the LEEs, namely, the acoustic waves, the entropy mode, and the vorticity mode. Two mean flow configurations have been investigated: in Sec. V, only acoustic perturbations can develop with the chosen parameters, and in Sec. VI, instability waves can also develop.

V. Source Radiation in a Sheared Mean Flow

Refraction effects strongly modify the directivity pattern of a source. As an example we consider the radiation of a source placed on the axis of a fully developed two-dimensional jet modeled with a Bickley's profile given in a dimensionless form by

$$u_0 = \frac{0.5}{\cosh^2[(1+\sqrt{2})y/b]} \tag{8}$$

The axial Mach number is $M = 0.5$, the half-width b of the jet is taken as $b = 10$, and the source term is again given by expression (4). The width of the source is $\alpha = \ell n\, 2/9$, the amplitude is $\epsilon = 0.01$, and the angular frequency is $\omega = 2\pi/9$. The wavelength of the source is of the same order of magnitude as the half-width of the jet producing strong refraction effects. This corresponds to a high-frequency radiation because the Strouhal number based on the jet diameter $D = 2b$ and the jet velocity $u_j = 0.5$ is $Sr = fD/u_j \simeq 4.4$. The same computational domain is used, but the source is now located at $x_s = -100$ and $y_s = 0$. The calculation is performed with CFL $= 1$, and the artificial selective damping is $R_s = 10$. Figure 9 shows the computed pressure field isocontours. The radiation pattern is strongly modified by the mean flow gradients. The acoustic level reaches a peak in the downstream direction near the angle θ given by the relation $\cos\theta = 1/(1+M)$. For smaller angles, the amplitude decreases, and a shadow zone is observed. In the upstream direction, acoustic waves are confined in the jet flow. The final time calculation corresponding to Fig. 9 is equal to 100 times the period of the acoustic wave, and the number of mesh points per wavelength is equal to 6 in the upstream direction and 14 in the downstream direction.

These results are in agreement with the geometrical acoustics approximation valid for high frequencies. Indeed, the ray-tracing equations[25] can be solved to obtain a reference solution. The ray tracing in Fig. 10 shows that the radiation features are well illustrated. The angle of the shadow zone, $\theta \approx 48$ deg, can be easily seen. From $0 \leq \theta \leq \pi$, 26 rays are plotted, and two wave fronts

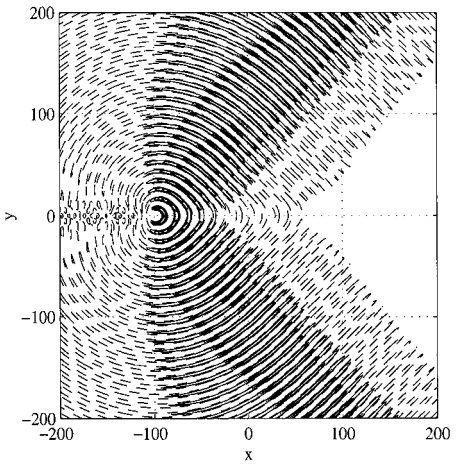

Fig. 9 Radiation of a source point in a sheared mean flow; instantaneous pressure contours at time $t = 900$: ——, isolines from 0.001 to 0.01 (increment 0.001), and – – –, isoline 10^{-4}.

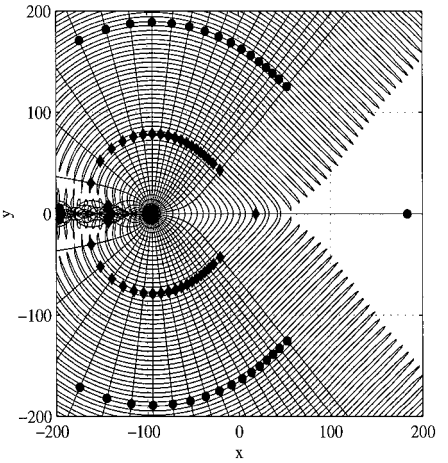

Fig. 10 Ray tracing for the radiation of a point source in the sheared mean flow [Eq. (8)].

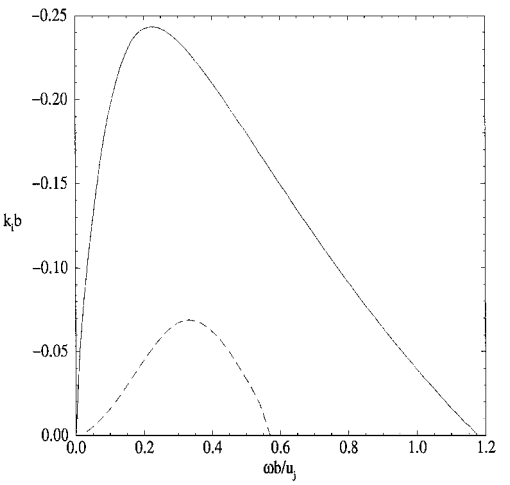

Fig. 11 Bickley jet profile (8): spatial growth rate $k_i b$ as a function of the frequency $\omega b/u_j$ for the sinuous mode (——) and the varicose mode (- - - -).

are marked by the symbol. The computed pressure field obtained by solving LEEs is superimposed on the ray-tracing plot, and excellent qualitative agreement is found. The radiation patterns of the two calculations are fully consistent. The wave fronts have the same characteristic oval shape without any difference in phase. A comparison of acoustic levels would be possible by computing the evolution of the ray tube cross section.[25] This would give some indications on the limit of application of geometrical acoustics as a function of the frequency. Thus, this example shows the good behavior of numerical algorithm (3).

It is well known that the LEEs support acoustic, entropy, and vorticity modes. The vorticity mode is generated by instability waves that may develop in the presence of acoustic sources in a sheared flow. In our case, the sinuous mode and the varicose mode of the Bickley jet [Eq. (8)] are not able to develop with the chosen value of the source frequency. The velocity perturbation can be described by a stream function $\psi(x, y, t) = \phi(y)e^{i(kx-\omega t)}$, where $k = k_r + ik_i \in \mathbb{C}$ is the complex wave number and $\omega \in \mathbb{R}$ is the angular frequency (see Fig. 11). Thus, these aerodynamic perturbations grow when the imaginary part of k is negative. The spatial growth rate $k_i b$ of the perturbations is plotted as a function of the frequency parameter $\omega b/u_j$ in Fig. 11. The two curves are obtained by solving the Rayleigh stability equation[26] with symmetric and antisymmetric boundary conditions yielding the stability characteristics of the sinuous mode and the varicose mode, respectively. Figure 11 shows that the reduced frequency is too high in our case because the growth rate is positive $k_i b > 0$ for the value $\omega b/u_j \simeq 13.9$.

VI. Nonlinear Propagation

To observe instability waves and acoustic waves, the mean flow is chosen now in the form of an hyperbolic tangent profile:

$$u_0 = \tfrac{1}{2}(1 + \tanh\{(H/2\delta_\theta)[1 - (|y|/H)]\}) \tag{9}$$

where H is the thickness of the jet shear layer and δ_θ its momentum thickness. The slow divergence of real jet flows is not taken into account in this study, which is limited to a strictly parallel flow. These parameters are taken as $H = 9$ and $\delta_\theta = 1$. The angular frequency is $\omega = 2\pi/40$ and corresponds to a Strouhal number $Sr = fD/u_j \simeq 1.4$. The two shear layers of the jet profile [Eq. (9)] can be considered as independent because the ratio $\delta_\theta/H \leq 0.08$ is very small. Thus, the stability characteristics of a single hyperbolic tangent profile can be used. The frequency parameter is $\omega\delta_\theta/u_o \simeq 0.314$ yielding an axial wave number $2\delta_\theta k_r \simeq 0.678$, as shown in Fig. 12 (see Ref. 27). The corresponding theoretical wavelength is $\lambda_{\text{th}} \simeq 18.5$. The descriptions of the computational domain and the source term are identical to those provided in Sec. V. The time evolution of the pressure along $y = 0$ is plotted in Fig. 13 and shows the exponential growth of instability waves produced by the acoustic source term. The apparent or convected instability wavelength provided by the calculation is $\lambda_a \simeq 30$, which corresponds to a real wavelength λ such as $\lambda_a = (1 + M)\lambda$, that is, $\lambda \simeq 20$. Thus, this result is in good agreement with the linear stability theory.

A nonlinear formulation has been developed to saturate the growth of these instability waves. The linear propagation governed by Eqs. (2) becomes

$$\frac{\partial \boldsymbol{U}}{\partial t} + \frac{\partial \boldsymbol{E}}{\partial x} + \frac{\partial \boldsymbol{F}}{\partial y} + \frac{\partial \boldsymbol{E}_{\text{nl}}}{\partial x} + \frac{\partial \boldsymbol{F}_{\text{nl}}}{\partial y} + \boldsymbol{H} = \boldsymbol{S} \tag{10}$$

where the flux vectors $\boldsymbol{E}_{\text{nl}}$ and $\boldsymbol{F}_{\text{nl}}$ contain all of the nonlinear terms. The influence of nonlinear terms may be illustrated by the following example. If we assume that the perturbation velocity has the form $\psi(x, y, t) = \phi(y)\, e^{ik(x - ct)}$ with $(k, c) \in \mathbb{C}$, then the square of the perturbation amplitude $A = \psi\psi^\star$ satisfies the equation $\partial A/\partial t = 2kc_i A$, where $c = c_r + ic_i$. Perturbations are unstable if the imaginary part of the speed c is positive, that is, $c_i > 0$. The effect of including nonlinear terms may be seen in the following model equation:

$$\frac{\partial A}{\partial t} = 2kc_i A - bA^2$$

where b is a constant. The perturbation amplitude is then given by

$$1/A = b/2kc_i + \beta e^{-i2kc_i t}$$

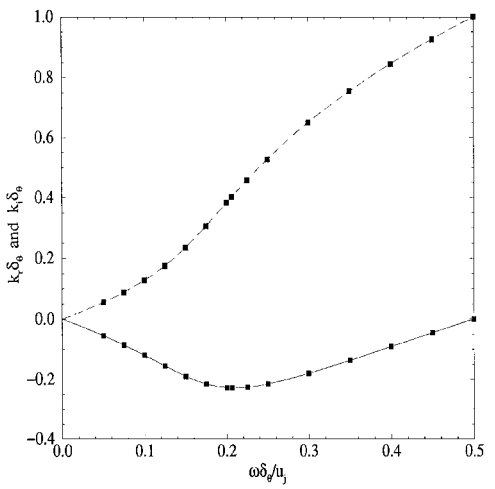

Fig. 12 Hyperbolic tangent profile $u = u_j[1 + \tanh(y/(2\delta_\theta)]$: real part of the wave number $2k_r\delta_\theta$ (- - - -), spatial growth rate $2k_i\delta_\theta$ (——) as a function of the frequency parameter $\omega\delta_\theta/u_j$, and values calculated by Michalke[27] symbols.

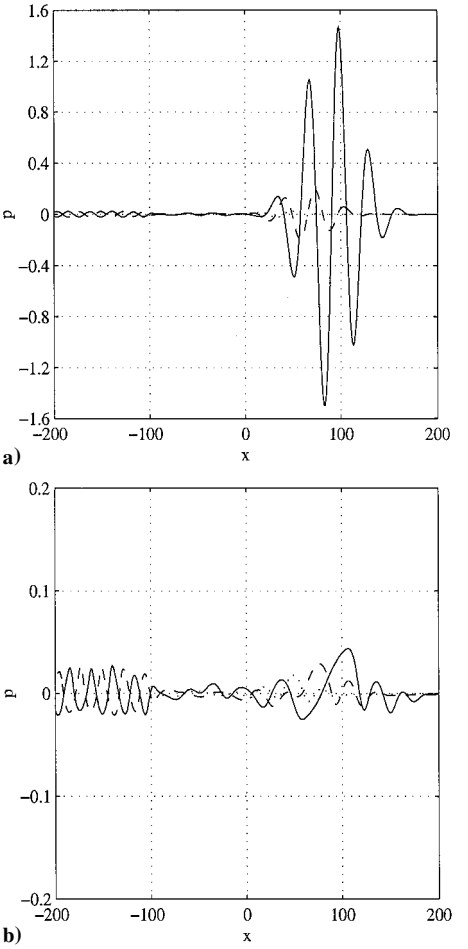

Fig. 13 Influence of the nonlinear terms; pressure profile plotted along the axis $y = 0$ at different time intervals: a) plot obtained without using the nonlinear terms [Eq. (2)] and b) plot obtained using the nonlinear terms [Eq. (10)], where · · · , $t = 600$; - - -, $t = 700$; and ——, $t = 800$.

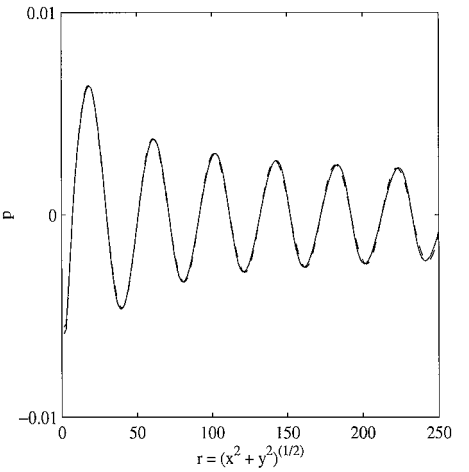

Fig. 14 Nonlinear formulation, comparison of the pressure profile along the line $x = y$ from the point source (x_s, y_s) at time $t = 500$: ——, with nonlinear terms, and - - - -, without nonlinear terms.

where β is an integration constant. Thus, the growth of the velocity perturbation is limited by taking into account nonlinear terms.

Figure 13b shows the pressure profile along the axis $y = 0$ obtained by solving Eq. (10). The time evolution of the pressure shows the signal deformation and wave form steepening due to nonlinear effects and the saturation of the growth of the instability waves. However, the nonlinear formulation does not change the radiated pressure field significantly. The pressure profiles along the line $x = y$ from the source point (x_s, y_s) are plotted in Fig. 14. No significant

difference is observed between numerical results obtained by solving Eqs. (2) and (10), respectively.

In these computations, the boundary conditions given in Sec. II are still used. However, instability waves are now convected by the mean flow, and better results should probably be obtained with the outflow boundary condition of Tam and Dong[28] for nonuniform mean flows.

VII. Conclusions

Computing sound propagation by solving the LEEs provides accurate solutions with very good performances in terms of stability, low storage, and computation time. Implementation of source terms has been investigated in various configurations, and the provided analytical solutions can be used to check accuracy of numerical simulations in CAA. In addition, the multipolar nature of the source is preserved by the numerical scheme, a crucial point for aerodynamic noise predictions. The growth of instability waves that are supported by LEEs can be limited by taking into account nonlinear terms without altering the evaluation of sound waves. All of the results presented have been obtained with a two-dimensional geometry. An extension of the propagation code to three dimensions has been recently achieved, and the SNGR model is currently being used to compute the noise radiated by a subsonic jet.

Appendix: Analytical Solutions

We briefly derive the analytic expression of the radiation of an harmonic monopole source in a subsonic or supersonic uniform mean flow such as $(u_0, 0)$. The LEEs reduce to

$$\frac{\mathrm{d}\boldsymbol{u}'}{\mathrm{d}t} + \frac{1}{\rho_0}\nabla p' = 0 \qquad \frac{\mathrm{d}p'}{\mathrm{d}t} + \gamma p_0 \nabla\cdot\boldsymbol{u}' = 0 \qquad \text{where} \quad \frac{\mathrm{d}}{\mathrm{d}t} = \frac{\partial}{\partial t} + u_0\frac{\partial}{\partial x} \tag{A1}$$

The wave equation associated to this system for Green's function $\mathcal{G}$ is

$$\frac{\mathrm{d}^2\mathcal{G}}{\mathrm{d}t^2} - c_0^2\nabla^2\mathcal{G} = \delta(x, y)e^{-i\omega t}$$

To solve this equation, we introduce a coordinate system moving with the mean flow. By setting $\tilde{t} = t$, $\tilde{x} = x - u_0 t$, and $\tilde{y} = y$, the wave equation becomes

$$\frac{\partial^2\tilde{\mathcal{G}}}{\partial\tilde{t}^2} - c_0^2\nabla^2\tilde{\mathcal{G}} = \delta(\tilde{x} + u_0\tilde{t}, \tilde{y})e^{-i\omega\tilde{t}}$$

where $\tilde{\mathcal{G}}(\tilde{x}, \tilde{y}, \tilde{t}) = \mathcal{G}(x, y, t)$. Thus, the exact solution can be constructed by introducing the two-dimensional free-space Green function. With the primitive variables, one finds

$$\mathcal{G}(x, y, t) = \frac{e^{-i\omega t}}{2\pi c_0}\int_D \frac{e^{i\omega\tau}}{\sqrt{c_0^2\tau^2 - (x - u_0\tau)^2 - y^2}}\,\mathrm{d}\tau \tag{A2}$$

where the integral is defined over the domain D:

$$D = \left\{ g(\tau) = \tau^2 - \frac{(x - u_0\tau)^2 + y^2}{c_0^2} > 0 \text{ and } \tau \geq 0 \right\}$$

To perform the integration of Eq. (A2), we have to determine the sign of the two roots τ^- and τ^+, with $\tau^- \leq \tau^+$, of the polynomial $g(\tau)$, as a function of the Mach number $M = u_0/c_0$. For a subsonic mean flow, $M < 1$, the function g can be factorized as $g(\tau) = (1 - M^2)(\tau - \tau^+)(\tau - \tau^-)$, where the two roots are given by

$$\tau^{\pm} = \frac{1}{c_0}\frac{-xM \pm \sqrt{x^2 + (1 - M^2)y^2}}{1 - M^2}$$

The integration is carried out over the domain $D = [\tau^+, \infty[$. This interval of integration can be made symmetrical by introducing the new variable s such that

$$\tau = \frac{\tau^+ - \tau^-}{2}s + \frac{\tau^+ + \tau^-}{2}$$

Thus, with the use of an integral representation[29] of the zeroth-order Hankel function of the first kind $H_0^{(1)}$, we have

$$\begin{aligned}\mathcal{G}(x, y, t) &= \frac{\exp(-i\omega t)}{2\pi c_0^2\sqrt{1 - M^2}}\exp\left(i\omega\frac{\tau^+ + \tau^-}{2}\right)\\ &\quad\times\int_1^{\infty}\exp\left(i\omega\frac{\tau^+ - \tau^-}{2}s\right)\frac{\mathrm{d}s}{\sqrt{s^2 - 1}}\\ &= \frac{\exp(-i\omega t)}{2\pi c_0^2\sqrt{1 - M^2}}\exp\left(i\omega\frac{\tau^+ + \tau^-}{2}\right)\\ &\quad\times\int_0^{\infty}\exp\left(i\omega\frac{\tau^+ - \tau^-}{2}\cosh u\right)\mathrm{d}u\\ &= \frac{\exp(-i\omega t)}{2\pi c_0^2\sqrt{1 - M^2}}\exp\left(i\omega\frac{\tau^+ + \tau^-}{2}\right)\frac{i\pi}{2}H_0^{(1)}\left(\omega\frac{\tau^+ - \tau^-}{2}\right)\end{aligned}$$

It can be shown that

$$\begin{aligned}\mathcal{G}(x, y, t) &= \frac{i}{4}\frac{1}{c_0^2\sqrt{1 - M^2}}H_0^{(1)}\left[k\frac{\sqrt{x^2 + (1 - M^2)y^2}}{1 - M^2}\right]\\ &\quad\times\exp\left(-i\frac{M}{1 - M^2}kx - i\omega t\right)\end{aligned} \tag{A3}$$

For a supersonic mean flow, $M > 1$, the function g can be written now as $g(\tau) = (M^2 - 1)(\tau^+ - \tau)(\tau - \tau^-)$ yielding the integration domain $[\tau^-, \tau^+]$ for the integral (A2). As in the subsonic case, by the introducing of an integral representation[29] of the Bessel function of zero order, J_0, one finds

$$\begin{aligned}\mathcal{G}(x, y, t) &= \frac{\exp(-i\omega t)}{2\pi c_0^2\sqrt{M^2 - 1}}\exp\left(i\omega\frac{\tau^+ + \tau^-}{2}\right)\\ &\quad\times\int_{-1}^{+1}\exp\left(i\omega\frac{\tau^+ - \tau^-}{2}s\right)\frac{\mathrm{d}s}{\sqrt{1 - s^2}}\\ &= \frac{\exp(-i\omega t)}{\pi c_0^2\sqrt{M^2 - 1}}\exp\left(i\omega\frac{\tau^+ + \tau^-}{2}\right)\\ &\quad\times\int_0^{\pi/2}\cos\left(\omega\frac{\tau^+ - \tau^-}{2}\cos\theta\right)\mathrm{d}\theta\\ &= \frac{\exp(-i\omega t)}{\pi c_0^2\sqrt{M^2 - 1}}\exp\left(i\omega\frac{\tau^+ + \tau^-}{2}\right)\frac{\pi}{2}J_0\left(\omega\frac{\tau^+ - \tau^-}{2}\right)\end{aligned}$$

Hence, Green's function is

$$\begin{aligned}\mathcal{G}(x, y, t) &= \frac{1}{2}\frac{1}{c_0^2\sqrt{M^2 - 1}}J_0\left[k\frac{\sqrt{x^2 - (M^2 - 1)y^2}}{M^2 - 1}\right]\\ &\quad\times\exp\left(-i\frac{M}{M^2 - 1}kx - i\omega t\right)\end{aligned} \tag{A4}$$

for the points located in the Mach cone $\mathcal{C}$ defined as

$$\mathcal{C} = \{(x, y) \in \mathcal{D}/x^2 - (M^2 - 1)y^2 \leq 0 \text{ and } x \leq 0\}$$

A more classical expression of $\mathcal{C}$ in cylindrical coordinates is $M\sin\theta > 0$, where θ is the angle between the x axis and the observer. There is no radiation outside the cone $\mathcal{D}$.

Expressions (A3) and (A4) are in agreement with those provided by Candel and Crance[22] for a similar radiation problem. We now consider a source term in the continuity equation of LEEs (11):

$$\frac{\mathrm{d}\boldsymbol{u}'}{\mathrm{d}t} + \frac{1}{\rho_0}\nabla p' = 0, \qquad \frac{\mathrm{d}p'}{\mathrm{d}t} + \gamma p_0\nabla\cdot\boldsymbol{u}' = Q$$

where $Q = f(x, y)\,e^{-i\omega t}$. The expression of the radiated pressure field is then obtained by the space convolution product $p = f \times \mathrm{d}\mathcal{G}/\mathrm{d}t$, where Green's function $\mathcal{G}$ has been calculated for a subsonic [Eq. (A3)] and a supersonic [Eq. (A4)] mean flow.

Acknowledgments

Computing time was provided by Institut du Développement et des Ressources en Informatique Scientifique–Centre National de la Recherche Scientifique. Part of this work was also supported by the Centre National des Etudes Spatiales.

References

[1]Tam, C. K. W., "Computational Aeroacoustics: Issues and Methods," *AIAA Journal*, Vol. 33, No. 10, 1995, pp. 1788–1796.

[2]Lele, S. K., "Computational Aeroacoustics: A Review," AIAA Paper 97-0018, Jan. 1997.

[3]Lighthill, M. J., "On Sound Generated Aerodynamically—I. General Theory," *Proceedings of the Royal Society of London, Series A: Mathematical and Physical Sciences*, Vol. 211, No. 1107, 1952, pp. 564–587.

[4]Van Herpe, F., Lafon, P., and Crighton, D., "Noise Generation by Turbulent Flow in a Duct Obstructed by a Diaphragm," AIAA Paper 95-035, May 1995.

[5]Lilley, G. M., "The Generation and Radiation of Supersonic Jet Noise. Vol. IV—Theory of Turbulence Generated Jet Noise, Noise Radiation from Upstream Sources, and Combustion Noise. Part II: Generation of Sound in a Mixing Region," U.S. Air Force Aero-Propulsion Lab., AFAPL-TR-72-53, Vol. 4, 1972.

[6]Viswanathan, K., and Sankar, L. N., "Toward the Direct Calculation of Noise: Fluid/Acoustic Coupled Simulation," *AIAA Journal*, Vol. 33, No. 12, 1995, pp. 2271–2279.

[7]Mankbadi, R. R., Hixon, R., Shih, S. H., and Povinelli, L. A., "Use of Linearized Euler Equations for Supersonic Jet Noise Prediction," *AIAA Journal*, Vol. 36, No. 2, 1998, pp. 140–147.

[8]Morris, P. J., Wang, Q., Long, L. N., and Lockard, D. P., "Numerical Predictions of High Speed Jet Noise," AIAA Paper 97-1598, May 1997.

[9]Morris, P. J., Long, L. N., Scheidegger, T. E., Wang, Q., and Pilon, A. R., "High Speed Jet Noise Simulations," AIAA Paper 98-2290, June 1998.

[10]Tam, C. K. W., "Supersonic Jet Noise," *Annual Review of Fluid Mechanics*, Vol. 27, 1995, pp. 17–43.

[11]Hardin, J. C., and Pope, D. S., "Sound Generation by a Stenosis in a Pipe," *AIAA Journal*, Vol. 30, No. 2, 1992, pp. 312–317.

[12]Béchara, W., Bailly, C., Lafon, P., and Candel, S., "Stochastic Approach to Noise Modeling for Free Turbulent Flows," *AIAA Journal*, Vol. 32, No. 3, 1994, pp. 455–463.

[13]Bailly, C., Lafon, P., and Candel, S., "A Stochastic Approach to Compute Noise Generation and Radiation of Free Turbulent Flows," AIAA Paper 95-092, June 1995.

[14]Bailly, C., Lafon, P., and Candel, S., "Computation of Noise Generation and Propagation for Free and Confined Turbulent Flows," AIAA Paper 96-1732, May 1996.

[15]Lafon, P., "Computational of Wave Propagation in a Complex Flow," *Workshop on Benchmark Problems in Computational Aeroacoustics*, edited by J. C. Hardin, J. R. Ristorcelti, and C. K. W. Tam, NASA CP 3300, 1995, pp. 125–132.

[16]Tam, C. K. W., and Webb, J. C., "Dispersion-Relation-Preserving Finite Difference Schemes for Computational Acoustics," *Journal of Computational Physics*, Vol. 107, Aug. 1993, pp. 262–281.

[17]Tam, C. K. W., and Shen, H., "Direct Computation of Nonlinear Acoustic Pulses Using High-Order Finite Difference Schemes," AIAA Paper 93-4325, Oct. 1993.

[18]Hu, F. Q., Hussaini, M. Y., and Manthey, J. L., "Low-Dissipation and Low-Dispersion Runge–Kutta Schemes for Computational Acoustics," *Journal of Computational Physics*, Vol. 124, Jan. 1996, pp. 177–191.

[19]Bailly, C., Thévenin, R., and Juvé, D., "Numerical Simulation of Sound Source Radiation in Flows," *Theoretical and Computational Acoustics '97*, World Scientific, Singapore, 1999, pp. 595–608.

[20]*Workshop on Benchmark Problems in Computational Aeroacoustics*, edited by J. C. Hardin, J. R. Ristorcelli, and C. K. W. Tam, NASA CP 3300, 1995.

[21]*Second Computational Aeroacoustics Workshop on Benchmark Problems*, edited by C. K. W. Tam, and J. C. Hardin, NASA CP 3352, 1997.

[22]Candel, S. M., and Crance, C., "Direct Fourier Synthesis of Waves: Application to Acoustic Source Radiation," *AIAA Journal*, Vol. 19, No. 3, 1981, pp. 290–295.

[23]Crighton, D., "Basic Principles of Aerodynamic Noise Generation," *Progress in Aerospace Sciences*, Vol. 16, No. 1, 1975, pp. 31–96.

[24]Grèverie, L., and Bailly, C., "Construction d'un opérateur de propagation à partir des équations d'Euler linéarisées," *Comptes Rendus de l'Académie des Sciences, Paris, Serie IIb*, Vol. 326, No. 11, 1998, pp. 741–746.

[25]Candel, S. M., "Numerical Solution of Conservation Equations Arising in Linear Wave Theory: Application to Aeroacoustics," *Journal of Fluid Mechanics*, Vol. 83, No. 3, 1977, pp. 465–493.

[26]Drazin, P. G., and Reid, W. H., *Hydrodynamic Instability*, paperback ed., Cambridge Univ. Press, Cambridge, England, U.K., 1981; reprinted in 1997, p. 126.

[27]Michalke, A., "On Spatially Growing Disturbances in an Inviscid Shear Layer," *Journal of Fluid Mechanics*, Vol. 23, No. 3, 1965, pp. 521–544.

[28]Tam, C. K. W., and Dong, Z., "Radiation and Outflow Boundary Conditions for Direct Computation of Acoustic and Flow Disturbances in a Nonuniform Mean Flow," *Journal of Computational Acoustics*, Vol. 4, No. 2, 1996, pp. 175–201.

[29]Watson, G. N., *Theory of Bessel Functions*, 2nd paperback ed., Cambridge Univ. Press, Cambridge, England, U.K., 1966, pp. 36, 180.

P. J. Morris
Associate Editor